Supporting information

Synergistic Mechanisms of Boron-Doped Heptazine/Triazine Homojunction in Polymeric Carbon Nitride for Efficient Photocatalytic H_2O_2 Evolution

Chengqun Xu [a,d,*], Wenjie Zheng [a], Xiaolu Liu [b], Jie Li [a], Weipeng Lai [a], Xiaoying Liang [a], Yifan Chen [a], Donghua Fan [a], Hui Pan [b,c,*]

[a]School of Applied Physics and Materials, Wuyi University, Jiangmen 529020, P. R. China. E-mail: xuchengqun2019@yeah.net

[b]Institute of Applied Physics and Materials Engineering, University of Macau, Macao SAR, 999078, P. R. China. E-mail: huipan@um.edu.mo

[c]Department of Physics and Chemistry, Faculty of Science and Technology, University of Macau, Macao SAR, 999078, P. R. China

[d]International Center for Materials Nanoarchitectonics (WPI-MANA), National Institute for Materials Science (NIMS), 1-1 Namiki, Tsukuba, Ibaraki 305-0044, Japan.

Characterizations

The crystal structure of the prepared samples was recorded by X-ray diffraction (XRD, Bruker D8 Advanced diffractometer, CuKα radiation) and Fourier transform infrared (FTIR, PerkinElmer spectrometer) spectroscopy. The chemical state and elemental composition were investigated by X-ray photoelectron spectroscopy (XPS, Thermo Scientific ESCALAB 250) and elemental analysis (VARIO EL CUBE microanalyzer). The morphology and microstructure were collected by JEM-2100 F transmission electron microscopy (TEM) and Hitachi SU 8220 scanning electron microscopy (SEM). The ultraviolet-visible diffuse reflectance spectra (UV-vis DRS) were measured using a UV-3600 plus UV-vis-NIR spectrophotometer with $BaSO_4$ as the reference. Solid-state ^{13}C and ^{11}B nuclear magnetic resonance (NMR) was recorded by a JEOL 600M spectrometer. The BET specific surface area and N_2 adsorption-desorption isotherms were collected by Micromeritics TriStar II 3020. Electron paramagnetic resonance (EPR) singles of spin-trapped paramagnetic species with 5,5-dimethyl-1-pyrroline N-oxide (DMPO, methanol solution) and 2,2,6,6-tetramethylpiperidin-4-amine (TEMP, methanol solution) were performed on Bruker ELEXSYS E500 spectrometer. The oxygen temperature programmed desorption (O_2-TPD) was measured on a TP-5060. The photoluminescence (PL) spectra were obtained at room temperature by a fluorescence spectrophotometer (FLS-980). Moreover, electrochemical measurement was performed using a three-electrode quartz cell on a CHI 660 C electrochemical workstation (Shanghai Chenhua, China).

Photoelectrochemical property

The photocurrent was measured on a CHI 660C electrochemical workstation (Shanghai, China) using a conventional three-electrode cell, a Pt plate and an Ag/AgCl electrode as counter electrode and reference electrode, respectively. Na_2SO_4 (0.5 mol/L) was used as the electrolyte solution. The working electrode was prepared according to the following process; FTO glass substrate was cleaned by sonication successively with distilled water, acetone and ethanol for 60 min. Meanwhile, 0.10 g of ethocel (EC) was dissolved in 25 mL of ethanol by ultrasonic dispersion. Then, 5 mg of sample (MCN, MCN-200B, MCN-LiK and MCN-*x*B-LiK) was ultrasonically dispersed in the aforementioned ethanol of 0.5 mL with EC solution. The resulting dispersion was applied dropwise onto the FTO substrate. The electrodes were sealed with epoxy resin except for the 1 cm^2 sample area used for photoexcitation experiment. The sample electrodes were dried in air before test. The Electrochemical impedance spectroscopy (EIS) was tested at a bias voltage of 0.2 V vs Ag/ AgCl with an AC voltage of 5 mV in the dark. The frequency range were set between 1×10^{-2} and 1×10^{5} Hz. The photocurrent was operated using a 300 W Xe lamp (PLS-FX300HU, Beijing Perfectlight Technology Co. Ltd., China) equipped with a 420 nm cutoff filter.

Rotating disk electrode (RDE) measurements were also investigated by Chenhua CHI 760E electrochemical workstation with standard three electrodes. Similarly, the Pt wire and Ag/AgCl electrode were used as counter electrode and reference electrode, respectively. The preparation process of working electrode is as follows: 5 mg of as-prepared catalysts were evenly dispersed into 1 mL ethanol solution containing 10 vol%

Nafion. After that, 10 μL of above suspension was evenly dropped onto a clean glassy carbon electrode and used for testing after the sample drying naturally. The linear sweep voltammetry (LSV) was detected in 0.1 M phosphate buffer solution (pH= 7, O_2-saturated) with the scan rate of 10 mV/s. Simultaneously, the rotating speed of the working electrode was 400, 800, 1200, 1600 and 2000 rpm, respectively. And the transfer electron number (n) of O_2 reduction was calculated by the slopes of Koutecky-Levich plots with the following equation (1) and (2):

$$j^{-1}=j_k^{-1}+B^{-1}\omega^{-1/2} \quad (1)$$

$$B=0.2nFC_0D_0^{2/3}V^{-1/6} \quad (2)$$

Here, j means current density (mA/cm^2); j_k expresses the kinetic current density; ω is the angular velocity (rpm); F means Faraday constant (96485 C/mol); C_0 and D_0 are bulk concentration of O_2 (1.1×10^{-3} mol/cm^3) and diffusion coefficient of O_2 (1.1×10^{-5} cm^2/s), respectively. In addition, the v is dynamic viscosity of H_2O (0.01cm^2/s).

Computational details:

All calculations were performed using the plane-wave periodic DFT method in the Vienne ab initio simulation package (VASP) [1, 2]. The electron energies used the generalized gradient approximation in the Perdew-Burke-Ernzerhof (GGA-PBE) [3]. The projector augmented wave (PAW) method is used to describe the electron-ion interaction [4]. The cutoff energy was set as 400 eV to ensure the accurate energies. The Gaussian electron smearing method is used by $\sigma = 0.05$ eV. The vacuum layer was set as 15 Å to avoid interactions with other slabs [5]. T. A 3×3×1 Monkhorst-Pack k-point grid was used for sampling the Brillouin zone. The geometry optimization was done when the energy difference was lower than 10^{-5} eV and the convergence criterion on forces smaller than 0.05 eV/Å. The long-range van der Waals interactions were considered through the DFT-D3 scheme.

Photocatalytic hydrogen evolution (PHE)

In a typical PHE process, 50 mg of the catalyst was dispersed in 100 mL of solution containing 5 mL of $H_2PtCl_6 \cdot 6H_2O$ (3 wt% of Pt), 10 mL of TEOA and 85 mL of DI water in a Pyrex top-irradiation reaction vessel. The photocatalytic test was performed in an automatic reaction system (Labsolar-6A, Beijing Perfectlight) equipped with a gas chromatograph (Fuli GC9790SD). After degassing for 30 min to exclude air, the solution was exposed to a 300 W Xe lamp (PLS-SXE300D, $\lambda \geq 420$ nm) to perform the PHE reaction.

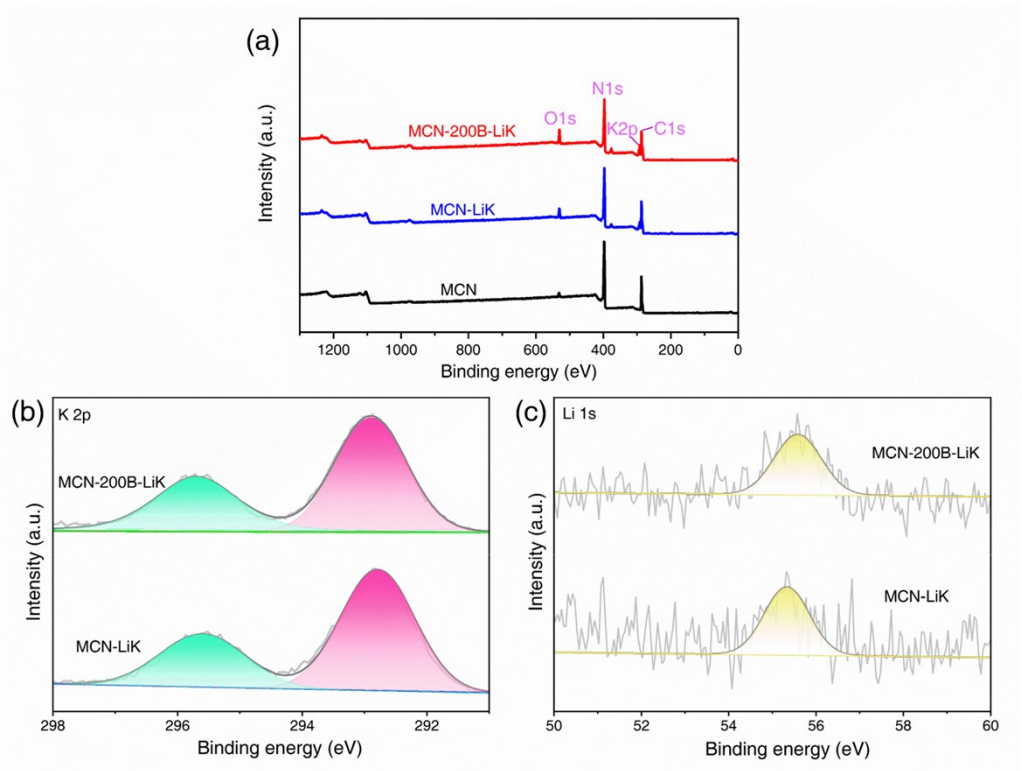

Figure S1. X-ray photoelectron spectra of the samples MCN, MCN-LiK and MCN-200B-LiK: (a) survey, (b) K 2p and (c) Li 1s;

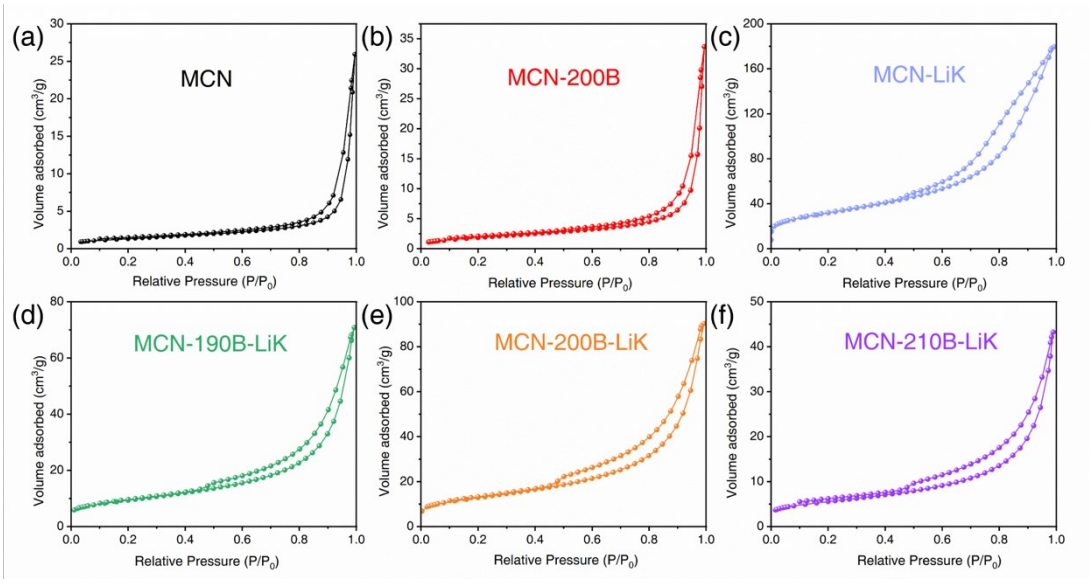

Figure S2. N_2 adsorption/desorption isotherms of MCN, MCN-200B, MCN-LiK and MCN-*x*B-LiK.

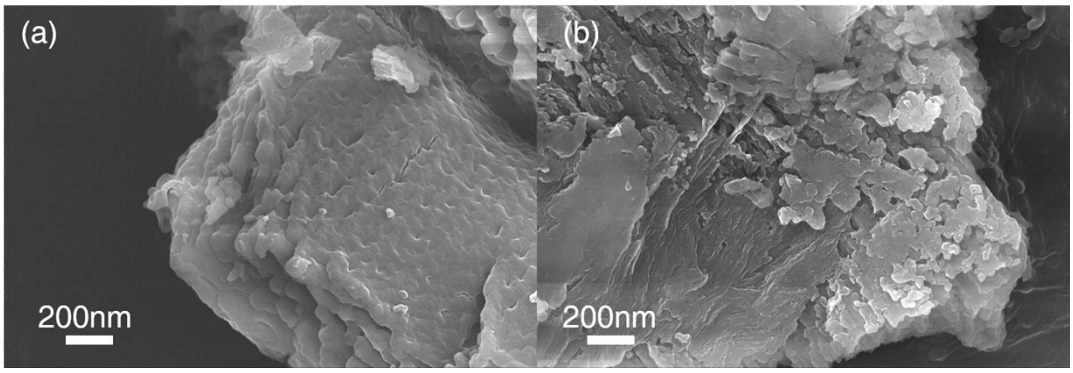

Figure S3. SEM images of the as-prepared (a) MCN and (b) MCN-200B.

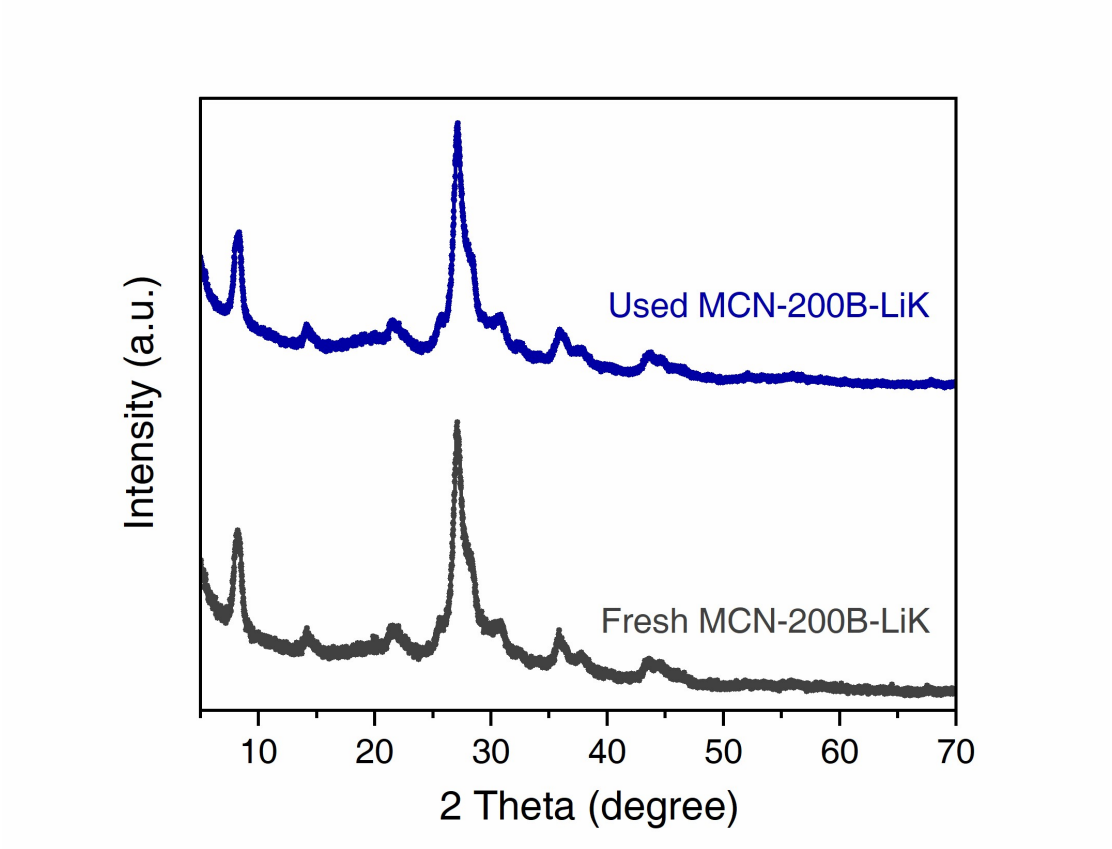

Figure S4. XRD patterns of MCN-200B-LiK after photocatalytic H_2O_2 evolution.

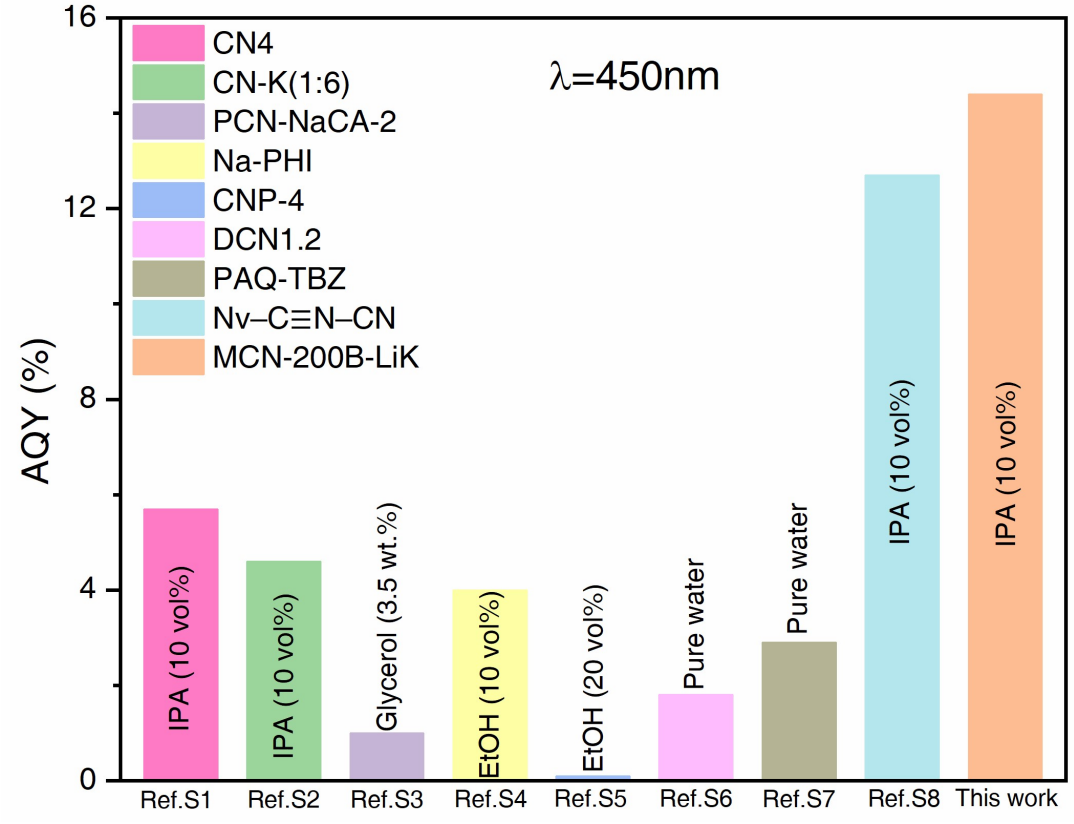

Figure S5. Comparison of wavelength-dependent AQY values for photocatalytic H_2O_2 production with those reported for PCN systems.

[6-13], as referred to as Ref. S1-S8.

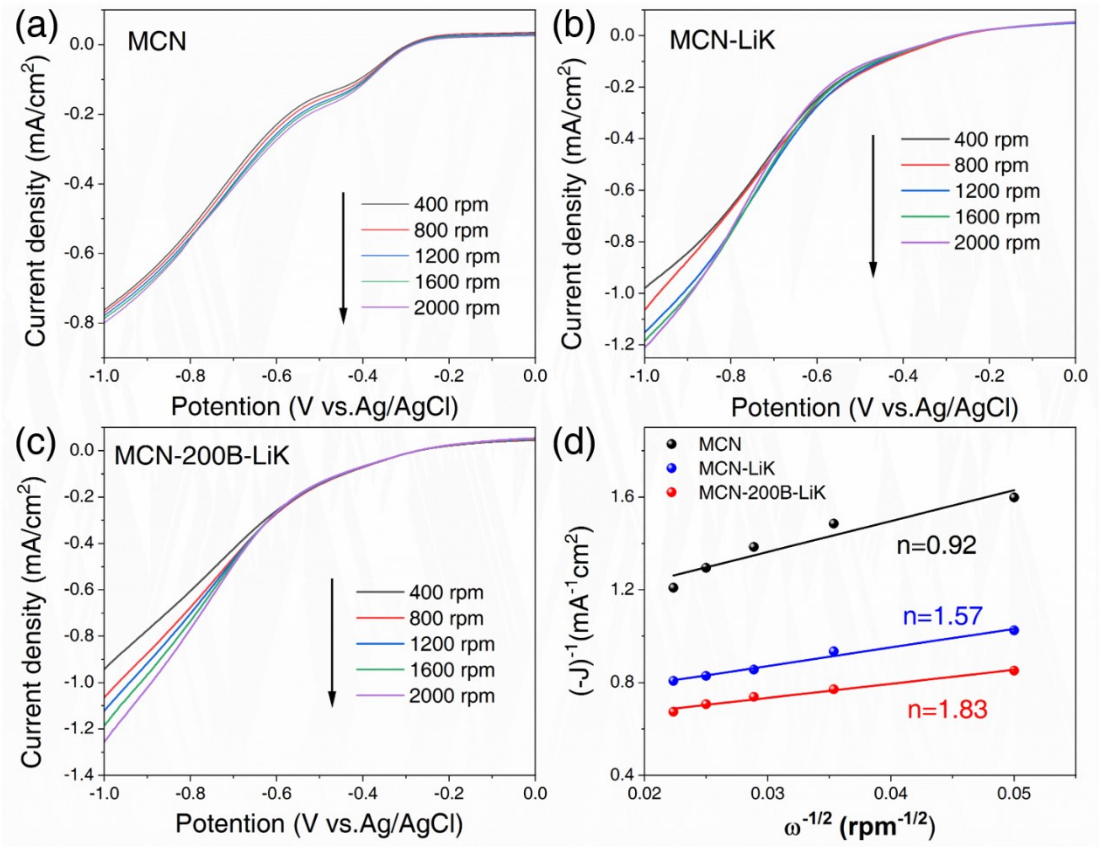

Figure S6. LSV curves of (a) MCN, (b) MCN-LiK and (c) MCN-200B-LiK measured on RDE at different rotating speeds; (d) Koutecky-Levich plots of MCN, MCN-LiK and MCN-200B-LiK.

Table S1. Summary of photocatalytic H_2O_2 production rates and their corresponding test conditions for previously reported PCN-based materials under visible light irradiation.

Catalysts	**Catalyst/ solution**	**Sacrificial agent**	**Light source**	**H_2O_2 yield ($\mu M \cdot L^{-1} \cdot h^{-1}$) $\cdot 10^3$**	**Ref.**
MCN-200B-LiK	50mg/50ml	10% isopropanol	$\lambda \geq 420$ nm	2.42	**This work**
CN-B-NV	30mg/30ml	3% isopropanol	$\lambda \geq 420$ nm	0.18	[14]
Leaf-vein-like CN	50mg/100ml	10% isopropanol	$\lambda \geq 420$ nm	0.28	[6]
CN-$NaSCN_{0.5}$	100mg/100 ml	10% ethanol	320nm< λ < 780 nm	0.11	[15]
O–CNC_4	50mg/50ml	10% isopropanol	AM 1.5G	2.0	[16]
KOH doped g-C_3N_4	25mg/50ml	10% isopropanol	/	0.02	[17]
KTTCN	30mg/30ml	0.5% isopropanol	$\lambda \geq 420$ nm	1.20	[18]
P-doped g-C_3N_4	10mg/15ml	/	420nm< λ < 700 nm	0.19	[19]
(K, P, O) doped g-C_3N_4	20mg/40ml	10% ethanol	$\lambda \geq 420$ nm	0.25	[20]
KPCN-x	50mg/100ml	10% isopropanol	320nm< λ < 780 nm	0.28	[21]
Nv-C≡N-CN	20 mg/20 ml	10% isopropanol	$\lambda \geq 420$ nm	3.10	[13]
NaB-CN	100 mg/100 ml	1% ethanol	$\lambda > 400$ nm	0.66	[22]

Reference:

[1] G. Kresse, J. Furthmüller, Efficiency of ab-initio total energy calculations for metals and semiconductors using a plane-wave basis set, Comp. Mater. Sci., 6 (1996) 15-50.

[2] G. Kresse, J. Furthmüller, Efficient iterative schemes for ab initio total-energy calculations using a plane-wave basis set, Phys. Rev. B, 54 (1996) 11169.

[3] J.P. Perdew, K. Burke, M. Ernzerhof, Generalized gradient approximation made simple, Phys. Rev. Lett., 77 (1996) 3865.

[4] G. Kresse, D. Joubert, From ultrasoft pseudopotentials to the projector augmented-

wave method, Phys. Rev. B, 59 (1999) 1758.
[5] T. Wang, S. Wang, Y. Li, J. Wang, H. Jiao, Adsorption equilibria of CO coverage on β-Mo_2C surfaces, J. Phys. Chem. C, 116 (2012) 6340-6348.
[6] C. Feng, L. Tang, Y. Deng, J. Wang, J. Luo, Y. Liu, X. Ouyang, H. Yang, J. Yu, J. Wang, Synthesis of leaf-vein-like g-C_3N_4 with tunable band structures and charge transfer properties for selective photocatalytic H_2O_2 evolution, Adv. Funct. Mater., 30 (2020) 2001922.
[7] W. Zhong, D. Zheng, Y. Ou, A. Meng, Y. Su, Simultaneously improving inter-plane crystallization and incorporating K atoms in g-C_3N_4 photocatalyst for highly-efficient H_2O_2 photosynthesis, Acta Phys. Chim. Sin, 40 (2024) 2406005.
[8] Y. Zhao, P. Zhang, Z. Yang, L. Li, J. Gao, S. Chen, T. Xie, C. Diao, S. Xi, B. Xiao, Mechanistic analysis of multiple processes controlling solar-driven H_2O_2 synthesis using engineered polymeric carbon nitride, Nat. Commun., 12 (2021) 3701.
[9] J. Yang, H. Yin, A. Du, M. Tebyetekerwa, C. Bie, Z. Wang, Z. Sun, Z. Zhang, X. Zeng, X. Zhang, Unveiling O_2 adsorption on non-metallic active site for selective photocatalytic H_2O_2 production, Appl. Catal. B: Environ. Energy, 361 (2025) 124586.
[10] X. Zhang, J. Yu, W. Macyk, S. Wageh, A.A. Al Ghamdi, L. Wang, C_3N_4/PDA S-Scheme heterojunction with enhanced photocatalytic H_2O_2 production performance and its mechanism, Adv. Sustain. Syst., 7 (2023) 2200113.
[11] Y. Shi, Q. Zhu, L. Fu, J. Wang, X. Lu, Y. Tao, C. Zhang, Y. Wang, K. Xu, H. Shang, Low-Coordinated Nitrogen Vacancies for Robust Visible-Light-Driven H_2O_2 Production, ACS EST Water, 5 (2024) 242-252.
[12] W. Chi, J. Wu, Y. Dong, J. Wu, Y. Zhu, Accelerated Exciton Dissociation and Charge Transfer via Third-Motif Engineered Conjugated Polymers for Photocatalytic Circulation-flow Synthesis of H_2O_2, Angew. Chem. Int. Edit., (2025) e202508690.
[13] X. Zhang, P. Ma, C. Wang, L. Gan, X. Chen, P. Zhang, Y. Wang, H. Li, L. Wang, X. Zhou, Unraveling the dual defect sites in graphite carbon nitride for ultrahigh photocatalytic H_2O_2 evolution, Energ. Environ. Sci., 15 (2022) 830-842.
[14] L. Zheng, Z. Wang, H. Zhang, Y. Shi, F. Wang, Z. Wang, D. Lin, J. Yue, Q. Wang, Boosting excitons dissociation in defective-rich graphitic carbon nitride for efficient hydrogen peroxide photosynthesis and on-site environmental governance, Appl. Catal. B: Environ. Energy, 347 (2024) 123811.
[15] H. Zhang, Z. Zhu, Y. Sun, M. Zuo, H. Zhou, Y. Chen, L. Han, NaSCN-Induced Cyano-Rich Porous Graphitic Carbon Nitride with Sodium Dopant and Nitrogen Vacancies for Enhanced Photosynthesis of Hydrogen Peroxide, Adv. Sustain. Syst., 8 (2024) 2400262.
[16] H. Xie, Y. Zheng, X. Guo, Y. Liu, Z. Zhang, J. Zhao, W. Zhang, Y. Wang, Y. Huang, Rapid microwave synthesis of mesoporous oxygen-doped g-C_3N_4 with carbon vacancies for efficient photocatalytic H_2O_2 production, ACS Sustainable Chem. Eng., 9 (2021) 6788-6798.
[17] H. Zhang, L. Jia, P. Wu, R. Xu, J. He, W. Jiang, Improved H_2O_2 photogeneration by KOH-doped g-C_3N_4 under visible light irradiation due to synergistic effect of

N defects and K modification, Appl. Surf. Sci., 527 (2020) 146584.
[18] J. Zhang, C. Yu, J. Lang, Y. Zhou, B. Zhou, Y.H. Hu, M. Long, Modulation of Lewis acidic-basic sites for efficient photocatalytic H_2O_2 production over potassium intercalated tri-s-triazine materials, Appl. Catal. B: Environ. Energy, 277 (2020) 119225.
[19] J. Cao, H. Wang, Y. Zhao, Y. Liu, Q. Wu, H. Huang, M. Shao, Y. Liu, Z. Kang, Phosphorus-doped porous carbon nitride for efficient sole production of hydrogen peroxide via photocatalytic water splitting with a two-channel pathway, J. Mater. Chem. A, 8 (2020) 3701-3707.
[20] G. Moon, M. Fujitsuka, S. Kim, T. Majima, X. Wang, W. Choi, Eco-friendly photochemical production of H_2O_2 through O_2 reduction over carbon nitride frameworks incorporated with multiple heteroelements, ACS Catal., 7 (2017) 2886-2895.
[21] Y. Pan, X. Liu, W. Zhang, B. Shao, Z. Liu, Q. Liang, T. Wu, Q. He, J. Huang, Z. Peng, Bifunctional template-mediated synthesis of porous ordered g-C_3N_4 decorated with potassium and cyano groups for effective photocatalytic H_2O_2 evolution from dual-electron O_2 reduction, Chem. Eng. J., 427 (2022) 132032.
[22] Y. Chu, X. Zheng, J. Fan, Preparation of sodium and boron co-doped graphitic carbon nitride for the enhanced production of H_2O_2 via two-electron oxygen reduction and the degradation of 2, 4-DCP via photocatalytic oxidation coupled with Fenton oxidation, Chem. Eng. J., 431 (2022) 134020.